Determination of mode i and mode II fracture toughness of walnut and cherry in TR and RT crack propagation system by the Arcan test

Author(s):
Murata, Koji; Bachtiar, Erik V.; Niemz, Peter

Publication date:
2017-11

Permanent link:
https://doi.org/10.3929/ethz-b-000219495

Originally published in:
Holzforschung 71(12), https://doi.org/10.1515/hf-2017-0063

Koji Murata*, Erik Valentine Bachtiar and Peter Niemz

Determination of mode I and mode II fracture toughness of walnut and cherry in TR and RT crack propagation system by the Arcan test

DOI 10.1515/hf-2017-0063
Received April 21, 2017; accepted June 19, 2017; previously published online July 26, 2017

Abstract: Two specimen types, each from walnut and cherry wood, were prepared for tangential-radial (TR) and radial-tangential (RT) crack propagation systems at 65% of RH and 20°C before mode I and mode II fracture toughness was determined through Arcan tests. It was found that fracture toughness in mode I is in agreement with literature data. In the mode II test, however, the crack propagated in the direction normal to the shear plane and not parallel to it. The release rate of strain energy in terms of the opening failure in mode II was lower than that in mode I. It can be concluded that it is difficult to determine the fracture toughness of RT or TR propagation in hardwood specimens in mode II.

Keywords: Arcan test, cherry, fracture toughness, walnut

Introduction

Natural forests are protected to maintain biodiversity and thus the harvesting of rare broadleaf trees (hardwoods, HWs) in such forests is forbidden worldwide. The Washington Convention prohibits the trade of rare HW species internationally. The furniture industry and manufacturers of musical instruments, the main consumers of rare HWs, are now looking for alternative HWs for their products as it is obvious that HWs in many applications cannot be substituted. Industrial wood-based products require for an optimal utilization the key mechanical parameters, such as Young's modulus (modulus of elasticity, MOE), Poisson's ratio, fracture toughness, the swelling and the shrinkage. Fracture toughness, in particular, plays a major role in almost every wood-related industrial process, e.g. in the context of cutting, connection, nailing, etc. However, past studies have focused more on the properties of softwood (SWs) than HWs. Therefore, the HWs cherry (*Prunus*) and walnut (*Juglans*), which play a pivotal role as materials for cultural heritage objects, are the focus of the present study.

Anisotropic wood is remarkably weak across the fiber direction. Aging, in particular, strongly affects the cleavage strength. Splitting caused by the drying process appears on the end surface of planks, and it can be the origin of a large fracture in case of HWs with high specific density. This is the reason why the crack development on the end surface in the mode I and II tests will be observed and the fracture toughness via end-surface specimens will be estimated. There are literature data concerning the fracture mechanics in the tangential-radial (TR) and radial-tangential (RT) systems (Ando and Ohta 1999; Ozyhar et al. 2012; Ozden and Ennos 2014; Tukiainen and Hughes 2016a,b; Özden et al. 2017) and it is reported that shear tests, such as the mode II tests, have several constraints. Looking for alternatives, the asymmetric four-point bending test and the Iosipescu test were investigated (Yoshihara et al. 1999; Yoshihara and Kubojima 2002). In the present paper the Arcan test, which can be considered as a relatively pure shear stress test suited to obtain fracture toughness, will be applied (Arcan et al. 1978).

Materials and methods

European walnut (*Juglans regra* L.) and cherry (*Prunus avium* L.) was grown in the Caucasus region in Eastern Europe; their average oven-dried densities were 631 and 506 kg m^{-3}, respectively. The dimensions of the specimens were 130 mm × 50 mm × 8 mm. A 24 mm long notch was cut by a mini-band saw, and final sharp notches of 0.5–1 mm were made with a razor blade. Two types of specimens were prepared, namely the RT and the TR speciments (Figure 1a), and conditioned at 65% relative humidity (RH) and 20°C. The random pattern for testing was sprayed with white and black ink on the surfaces of the specimens. Eight specimens (for each wood) were tested in mode I, and five specimens were tested in mode II (Table 1).

***Corresponding author: Koji Murata,** Graduate School of Agriculture, Kyoto University, Kitashirakawa-Oiwake cho, Sakyo ku, Kyoto city, Kyoto, 606-8502, Japan, e-mail: murata@kais.kyoto-u.ac.jp
Erik Valentine Bachtiar: Institute for Building Materials, ETH Zürich, Zürich, Switzerland
Peter Niemz: Institute for Building Materials, ETH Zürich, Zürich, Switzerland; and Institute for Material and Wood Technology, Bern University of Applied Sciences, Burgdorf, Switzerland

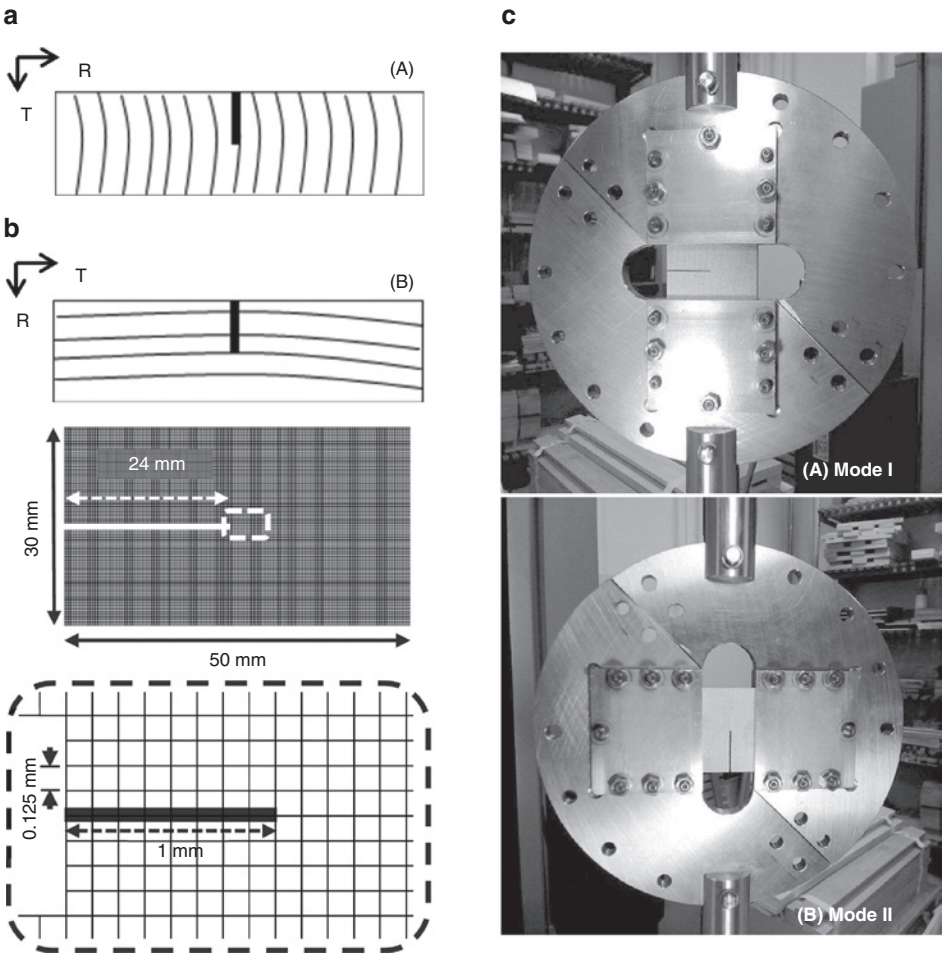

Figure 1: Experimental setups and a model of FEM analysis.
(a) Single-edge-notch specimen. (A) RT specimen, (B) TR specimen. (b) Specimen model in the FEM analysis. (c) Set up of Arcan test attachment.

Table 1: Average density (ρ) and moisture content (MC) of the specimens.

Parameters	Mode I	Mode II
RT, WN ρ (kg m^{-3})	612	603
RT, CH ρ (kg m^{-3})	532	527
RT, MC, WN (%)		9.9
RT, MC, CH (%)		10.2
TR, WN ρ (kg m^{-3})	664	672
TR, CH ρ (kg m^{-3})	489	494
TR, MC, WN (%)		8.9
TR, MC, CH (%)		11.2

WN, Walnut; CH, cherry.

The Arcan tests were conducted on a Zwick/Roell Z100 universal testing machine (Zwick GmbH & Co, Ulm, Germany), and an Arcan device was mounted in mode I and mode II test configuration (Figure 1c). The displacement rate was 1 mm min^{-1}, which leads to rupture in ca. 60 s. During the test, images of one side of the specimen were captured on a digital camera with a frequency of 2 Hz. These images were further analyzed to obtain the strain distribution on the specimen during the measurement. The fracture toughness (K_c) was calculated (Ammann and Niemz 2015):

$$K_{IC} = \zeta_I \cdot \frac{F_{max}}{w \cdot t} \sqrt{\pi \cdot a}, \quad (1)$$

$$K_{IIC} = \zeta_{II} \cdot \frac{F_{max}}{w \cdot t} \sqrt{\pi \cdot a}, \quad (2)$$

where K_c is the critical stress intensity factor; F_{max} is the critical load at which the crack begins to propagate; w and t are the width and the thickness of the specimen, respectively; a is the initial crack length; $\zeta_I = 2.810$ and $\zeta_{II} = 1.448$ are the correction factors of each formula.

The strain release energy for each mode was estimated via the virtual crack closure technique (VCCT) and the finite element method (FEM), in which a certain modulus of elasticity (MOE) and shear modulus was used. Bachtiar et al. (2017) determined the MOE data of the walnut and cherry specimens; the wood for the present study was from the same region (Table 2). The strain energy release rate for VCCT was calculated (Krueger 2004).

Table 2: Elastic moduli (E_R, E_T) and Poisson's ratio (μ_{TR} and μ_{RT}) (Bachtiar et al. 2017).

Data	Walnut	Cherry
E_R (MPa)	1083	885
E_T (MPa)	1049	1609
G_{TR} (MPa)	194	218
Poisson's ratio		
μ_{TR}[a]	0.524	0.734
μ_{RT}[a]	0.297	0.350

[a]First and second subscripts mean loading and lateral directions, respectively.

$$G_I = \frac{1}{2\Delta a} Y_1 \cdot \Delta v_2, \quad (3)$$

$$G_{II} = \frac{1}{2\Delta a} X_1 \cdot \Delta u_2, \quad (4)$$

where Δa is a finite crack extension in the FEM analysis, (X_1, Y_1) is a force vector on the crack-tip node before the crack extension (step 1), and (Δu_2, Δv_2) is a displacement vector after crack extension (step 2); X and u are the force and the displacement along the initial crack, respectively, and Y and v are across from it.

The FEM model is presented in Figure 1b. The final sharp notch of 1 mm was simulated as discontinuous elements with double nodes. The model in step 1 is shown in Figure 3. In step 2, the final sharp notch was extended by Δa in the direction where the specimen would break in a realistic experiment; thus, the modified model with Δa was simulated again. Constraint conditions in the FEM model were as follows: (1) Mode I: The upper support jig was loaded. The lower support jig was fixed in all displacement. The upper support jig was fixed without in the loading direction. Both jigs were not fixed in rotation, but a node in the center of the edge of the specimen on the opposite side of the notch was fixed in rotation. (2) Mode II: The right support jig was loaded. The left support jig was fixed in displacement and in rotation. The right support jig was fixed in displacement and in rotation except to move in the loading direction.

The FEM analyses were performed by the software MSC NASTRAN, version 70.0.6.

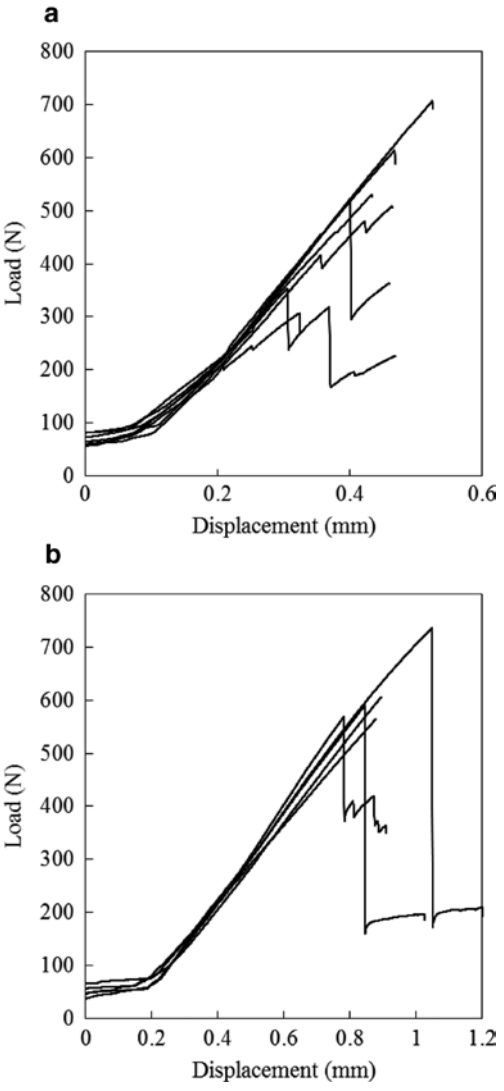

Figure 2: Typical load-displacement curves (cherry-TR system). (a) Model I test; (b) model II test.

Results and discussion

Typical load-displacement curves are presented in Figure 2. All specimens failed within the linear region, in a similar manner as brittle materials do. The maximum loads prior to the first load decrease were considered as critical loads in order to calculate the stress intensity factor. The obtained critical intensity factors are listed in Table 3. Vasic and Stanzel-Tschegg (2007) estimated the fracture toughness of SWs and HWs at different humidity levels, while beech and oak specimens (conditioned at 65% RH) were tested in micro-wedge-splitting tests. The K_{IC} in the TR system was estimated at 507 and 294 kPa $m^{0.5}$ for each type of specimen, respectively. Scheffler et al. (2004) measured the stress intensity factors of beech and oak wood types for several moisture contents (MCs) in the compact tension specimen. The results revealed that the values of K_{IC} of the TR and the RT system were 510 and 660 kPa $m^{0.5}$ for beech and 830 and 1200 kPa $m^{0.5}$ for oak (20°C and 65% RH), respectively. In Table 3, the K_{IC} values are slightly higher than those of the literature, although the species were different. Yoshihara and Kawamura (2007) compared four methods for measuring the mode I fracture toughness of wood. The equation in the quoted work for single edge notched tension (SENT) resulted in very similar fracture toughness data to those obtained by Eq. (1). Ammann and Niemz (2015) cited the correction factor from a previous report (Richard and Benitz 1983) where the species were not defined. The correction factor would

Table 3: Critical load F_c (N) and stress intensity factor K_c (kPa m$^{0.5}$) in the Arcan test in TR and RT direction in mode I and mode II.

Wood, parameters	F_c (kPa m$^{0.5}$)	K_c (kPa m$^{0.5}$)
Walnut		
TR I	607 (68)	1169 (133)
TR II	607 (68)	779 (64)
RT I	581 (61)	1453 (96)
RT II	789 (146)	782 (142)
Cherry		
TR I	467 (151)	876 (280)
TR II	467 (151)	593 (71)
RT I	780 (96)	1498 (244)
RT II	630 (63)	627 (631)

SD in parenthesis.

need a slight adjustment because of slightly different specimen shapes. The fracture process zone (FPZ) could be different in the literature and in the present study, but these differences can probably be neglected (Aicher 2010; Murata et al. 2011). Scheffler et al. (2004) concluded that the K_{IIC} values in the TR and the RT system were 580 and 410 kPa m$^{0.5}$, respectively. The results obtained in the present study are in fairly good agreement with the data of the quoted study.

Figure 3a shows the crack path after the failure of the specimen in the Arcan test. In the upper image, a crack expands along the initial notch. The crack path is in agreement with the hypothesis of finite crack expansion, and the stress intensity factor can be calculated from the stress field along the notch direction. In the bottom image, a crack is visible that has been generated in the normal direction to the shear plane, when the specimen started to fail. The crack gradually expanded toward the upper direction (parallel to the initial notch). The crack path indicates that a failure in the initial state did not appear as shear failure, and an opening failure occurred normal to the initial notch at the critical load. The shear failure [Eq. (2)] may not be suitable to describe this particular failure.

Figure 3b shows the strain distributions measured via the Vic-2D software (Correlated Solutions, Inc., SC, USA) in the mode I test. The concentration of the normal strain was found to be located 2–3 mm away from the tip of the initial notch. In this test, the normal stress near the tip caused a mode I failure. Figure 3c presents the strain distributions in the mode II test, where the concentration of

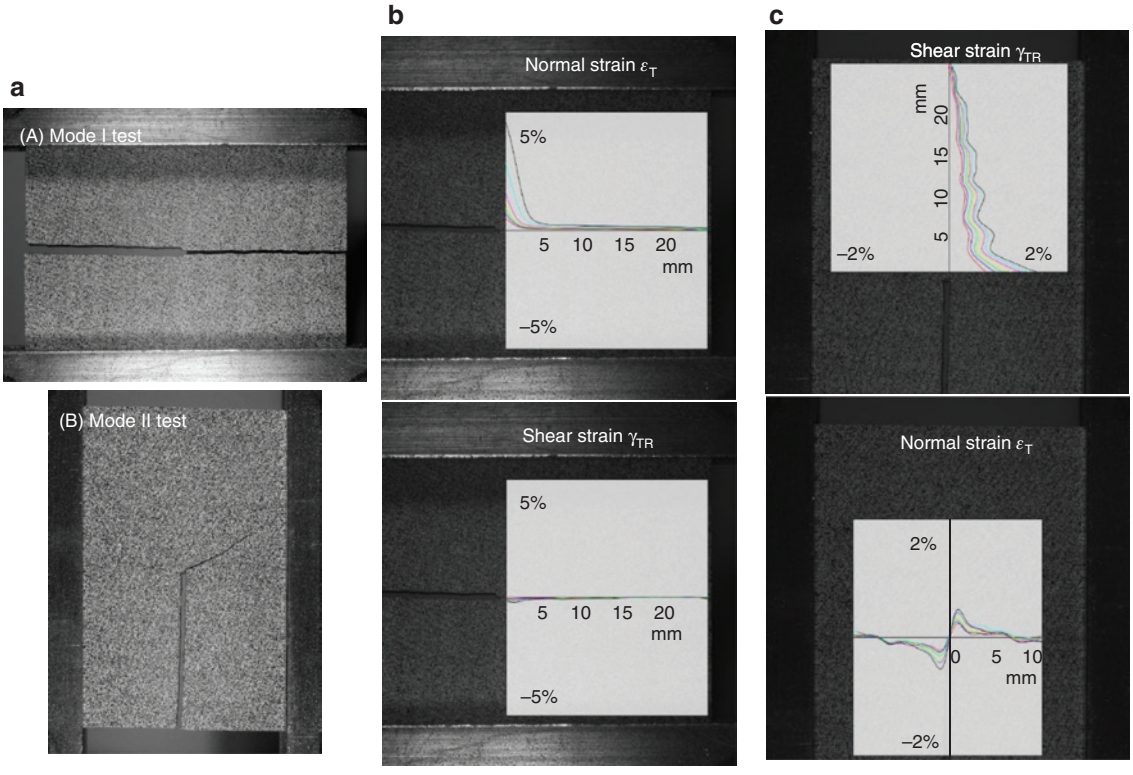

Figure 3: Strain distributions before fracture and crack path examples.
(a) Failures of the cherry specimen (TR) in the Arcan test. (b) Strain distribution (mode I test, cherry TR) from the tip, along the initial notch. The loads are 180, 235, 294, 355, 412, 465 and 521 N. (c) Strain distribution (mode II, cherry TR) from the tip; upper and lower image correspond to along and transverse to the initial notch, respectively. The loads are 332, 371, 411, 452, 590, 527 and 534 N.

the shear strain was found near the tip of the initial notch. However, the concentration of the normal strain was found to be slightly away from the tip in the horizontal direction (bottom image of Figure 3c). The positive normal strain must have been the reason for the opening failure in the mode II test.

The strain energy release rate was calculated using the VCCT. The critical load (maximum load) was applied in the presented model in Figure 1b, and a force vector (X_1, Y_1) on the tip of the initial notch was estimated via FEM. Then, the initial notch expanded by a finite crack Δa, and a displacement vector $(\Delta u_2, \Delta v_2)$ was estimated again (Figure 4). In this particular mode I test, the finite crack was generated in a direction parallel to the initial notch of Figure 4a. However, in the mode II test, the finite crack turned nearly 90° to the initial notch in Figure 4b. This can be interpreted such that the opening fracture (in mode I) occurred in this particular mode II test of the TR or RT system. Thus the coordinate system (X, Y) and (u, v) was rotated by 90° in Figure 4b, to calculate a strain release energy rate via Eqs. (3) and (4), respectively (Xie et al. 2004; Yoshihara 2013). Vasic and Stanzel-Tschegg (2007) measured the critical energy release rates of beech and oak specimens by micro-wedge-splitting tests. The values of G_{IC} of the TR system were estimated to be 682 and 229 J m^{-2} for each wood type, respectively. The simulated G_{IC} in the mode I test was obtained within adequate range by means of VCCT, although the data were slightly low. However, the specimen ruptured in the opening failure of the G_{IC} in the mode II test; nevertheless, the values of G_{IC} were significantly lower than those in mode I (Table 4). A similar failure mode occurred in both tests because of the opening failure. When a crack started to expand at a critical load, the strain energy release rate was equal to a crack resistance, creating new fracture surfaces according to linear elastic fracture mechanics (LEFM). It is not yet clarified why the G_{IC} in mode II was lower than that in mode I.

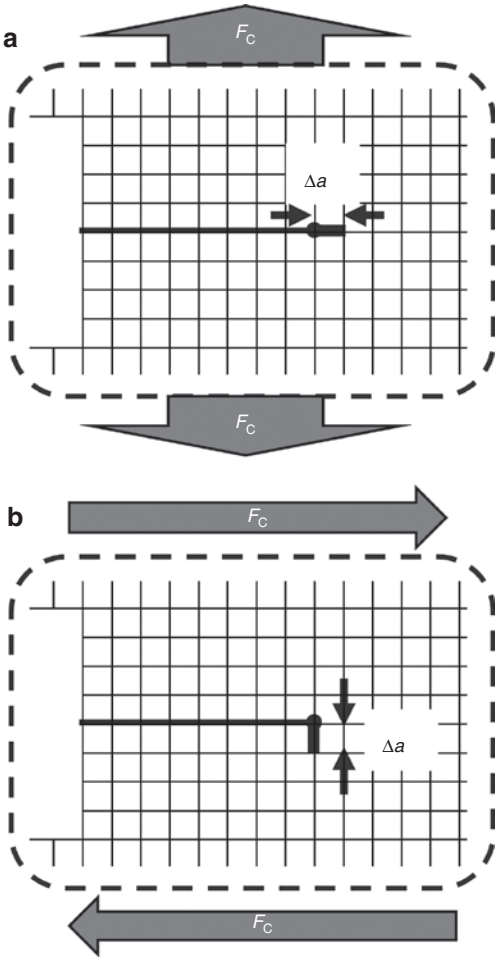

Figure 4: Finite crack expansion of the VCCT, (a): in the mode I test, (b) in the mode II test.

Table 4: Critical strain energy release rate G_{IC} in the Arcan test.

Wood, TR, RT	G_{IC} (J m^{-2})	
	Mode I	Mode II
WN, TR	190	79
WN, RT	285	77
CH, TR	110	42
CH, RT	248	64

Conclusion

The fracture toughness of the walnut and the cherry wood was measured via Arcan test. Single edge-notch specimens (SEN) for the TR and the RT crack propagation systems were acclimatized at 65% RH and 20°C. The stress intensity factor was calculated via an analytical equation, and the strain energy release rate was estimated through FEM, as well as by VCCT. The following results were obtained: (1) The SEN specimen of the TR and RT system failed similarly to a brittle material. In mode I, the initial notch expanded parallel to the direction of the notch direction; however, in the mode II test, a crack propagated in the normal direction to the shear plane. (2) In mode II, the stress intensity factor and the strain energy release rate were obtained within an acceptable range as observed in other works, although correction factors may be slightly adjusted. (3) In mode II, the analytical calculation was challenging because the crack

propagation direction was not in agreement with the hypothesis of a finite additional crack. The strain energy release rate of the opening crack was lower than that of the mode I test obtained by VCCT. The reason for this deviation is not yet investigated.

Acknowledgments: The authors would like to acknowledge the financial support of the Swiss National Science Foundation (SNF) project no. 147672 and Kyoto University Young Scholars Overseas Visit Program (The John Mung Program).

References

Aicher, S. (2010) Process zone length and fracture energy of spruce wood in mode-I from size effect. Wood Fib. Sci. 42:237–247.

Ammann, A., Niemz, P. (2015) Mixed-mode fracture toughness of bond lines of PRF and PUR adhesives in European beech wood. Holzforschung 69:415–420.

Ando, K., Ohta, M. (1999) Variability of fracture toughness by the crack tip position in an annual ring of coniferous wood. J. Wood Sci. 45:275–283.

Arcan, A., Hashin, Z., Voloshin, A. (1978) A method to produce uniform plane-stress states with applications to fiber-reinforced materials. Exp. Mech. 18:141–146.

Bachtiar, E.V., Sanabria, S.J., Mittig, J.P., Niemz, P. (2017) Mechanical behaviour of walnut (*Juglans regia* L.) and cherry (*Prunus avium* L.) wood in tension and compression in all anatomical directions. Revisiting the tensile/compressive stiffness ratios of wood. Available from: https://doi.org/10.1515/hf-2017-0053.

Krueger, R. (2004) Virtual crack closure technique: history, approach and applications. Appl. Mech. Rev. 57:109–143.

Murata, K., Nagai, H., Nakano, T. (2011) Estimation of width of fracture process zone in spruce wood by radial tensile test. Mech. Mater. 43:389–396.

Ozden, S., Ennos, A.R. (2014) Understanding the function of rays and wood density on transverse fracture behaviour of green wood in three species. J. Agr. Sci. Tech. B 4:731–743.

Özden, S., Slater, D., Ennos, R. (2017) Fracture properties of green wood formed within the forks of hazel (*Corylus avellana* L.). Trees 31:903–917.

Ozyhar, T., Hering, S., Niemz, P. (2012) Moisture-dependent elastic and strength anisotropy of European beech wood in tension. J. Mater. Sci. 47:6141–6150.

Richard, H.A., Benitz, K. (1983) A loading device for the creation of mixed mode in fracture mechanics. Int. J. Fract. 22:R55–R58.

Scheffler, M., Niemz, P., Diener, M., Lustig, V., Hardtke, H.-J. (2004) Fracture toughness from hardwood in mode I and II (in German). Holz Roh- Werkst. 62:93–100.

Tukiainen, P., Hughes, M. (2016a) The effect of temperature and moisture content on the fracture behaviour of spruce and birch. Holzforschung 70:369–376.

Tukiainen, P., Hughes, M. (2016b) The effect of elevated temperature and high moisture content on the fracture behaviour of thermally modified spruce. J. Mater. Sci. 51:1437–1444.

Vasic, S., Stanzel-Tschegg, S. (2007) Experimental and numerical investigation of wood fracture mechanisms at different humidity levels. Holzforschung 61:367–374.

Yoshihara, H., Ohsaki, H., Kubojima, Y., Ohta, M. (1999) Applicability of the Iosipescu shear test on the measurement of the shear properties of wood (in Japanese). J. Wood Sci. 45:24–29.

Yoshihara, H., Kubojima, Y. (2002) Measurement of the shear modulus of wood by asymmetric four-point bending tests. J. Wood Sci. 48:14–19.

Yoshihara, H., Kawamura, T. (2007) Influence of the measurement methods on the mode I fracture toughness of wood. J. Soc. Mater. Sci. Japan 56:311–315.

Yoshihara, H. (2013) Mode II critical stress intensity factor of medium-density fiberboard measured by asymmetric four-point bending tests and analyses of kink crack formation. BioResources 8:1771–1789.

Xie, D., Waas, A.M., Shahwan, K.W., Schroeder, J.A., Boeman, R.G. (2004) Computation of energy release rates for kinking cracks based on virtual crack closure technique. Comp. Model Eng. J. 6:515–524.